Substorm expansion triggered by a sudden impulse front propagating from the dayside magnetopause

K. Keika,[1] R. Nakamura,[1] W. Baumjohann,[1] V. Angelopoulos,[2] P. J. Chi,[2]
K. H. Glassmeier,[3,4] M. Fillingim,[5] W. Magnes,[1] H. U. Auster,[3] K. H. Fornaçon,[3]
G. D. Reeves,[6] K. Yumoto,[7] E. A. Lucek,[8] C. M. Carr,[8] and I. Dandouras[9]

[1]   We examine a substorm expansion on 21 June 2007, which occurred <2 min after a solar wind discontinuity accompanied by a dynamic pressure (P_d) increase impinged on the magnetopause. To investigate how the perturbation due to such P_d increase propagates in the magnetosphere and what the timing analysis may imply about how this type of substorms is triggered, we utilize a large number of in situ magnetic field and plasma observations, a remote sensing of auroral brightening, and ground-based magnetic field observations. The timing analysis shows that the front of a compression-associated sudden impulse can reach the substorm expansion onset site (dawnside near-Earth plasma sheet) at the substorm onset time. The onset site and time are determined from aurora images displaying aurora expansion, energetic electron data at geosynchronous orbit showing dispersed injection, and geomagnetic field data at high latitudes showing negative bays in the H component. Our 2-D calculations of the fast-mode propagation also demonstrate the arrival of the wavefront at the onset site and time. We suggest that for the class of substorms triggered by solar wind P_d increases, the triggering could occur within as short as 2 min after a P_d increase impinges on the magnetopause, consistent with the time needed for the sudden impulse wavefront to propagate inside the magnetosphere from the dayside magnetopause to the magnetotail.

1. Introduction

[2]   Sudden changes in the solar wind affect field and plasma phenomena in the magnetosphere and in the ionosphere [e.g., *Nishida*, 1978]. Although it is still a controversial issue whether a substorm is triggered externally by the sudden solar wind changes [e.g., *Aubry and McPherron*, 1971; *Burch*, 1972; *McPherron et al.*, 1986; *Lyons*, 1996] or internally by instabilities produced spontaneously in the plasma sheet [e.g., *Horwitz*, 1985; *McPherron et al.*, 1986;

Henderson et al., 1996], the major quantity responsible for the substorm triggering, in the concept of the external triggering, is the interplanetary magnetic field (IMF). Northward turning of IMF is one of the most significant changes [e.g., *Foster et al.*, 1971; *Pellinen et al.*, 1982; *Rostoker*, 1983]. On the other hand, a sudden increase in solar wind dynamic pressure (P_d) has been also considered to be another trigger of substorms [*Burch*, 1972; *Kokubun et al.*, 1977; *Iyemori and Tsunomura*, 1983; *Zhou and Tsurutani*, 2001; *Liou et al.*, 2003; *Lyons et al.*, 2005; *Meurant et al.*, 2005]. Statistical studies by *Liou et al.* [2003] using global auroral imaging indicate that the probability is low. *Lyons et al.* [2005] found that a P_d increase causes a substorm under steady, strongly southward IMF conditions.

[3]   Concerning the substorm triggering by a P_d increase, most studies identified the magnetospheric compression from a sudden enhancement in the H component of the geomagnetic field or/and in the Z component of the magnetic field in the inner magnetosphere, which is frequently termed a sudden impulse (SI) and is a consequence of the arrival of fast-mode waves excited at the magnetopause by the P_d increase. In order to identify the P_d effect, however, it is necessary to follow the propagation of the SI front inside the magnetosphere toward the magnetotail. In fact, the time differences between the SI onset and the substorm onset vary among substorms. *Iyemori and Tsunomura* [1983] showed the distribution of time differences between the SI onset on

[1]Space Research Institute, Austrian Academy of Sciences, Graz, Austria.
[2]Institute of Geophysics and Planetary Physics, University of California, Los Angeles, California, USA.
[3]Institut für Geophysik und Extraterrestrische Physik, Technische Universität Braunschweig, Braunschweig, Germany.
[4]Max Planck Institute of Solar System Research, Katlenburg-Lindau, Germany.
[5]Space Sciences Laboratory, University of California, Berkeley, California, USA.
[6]Los Alamos National Laboratory, Los Alamos, New Mexico, USA.
[7]Space Environment Research Center, Kyushu University, Fukuoka, Japan.
[8]Space and Atmospheric Physics Group, Imperial College, London, UK.
[9]Centre d'Etude Spatiale des Rayonnements, Université Paul Sabatier, UMR 5187, CNRS, Toulouse, France.
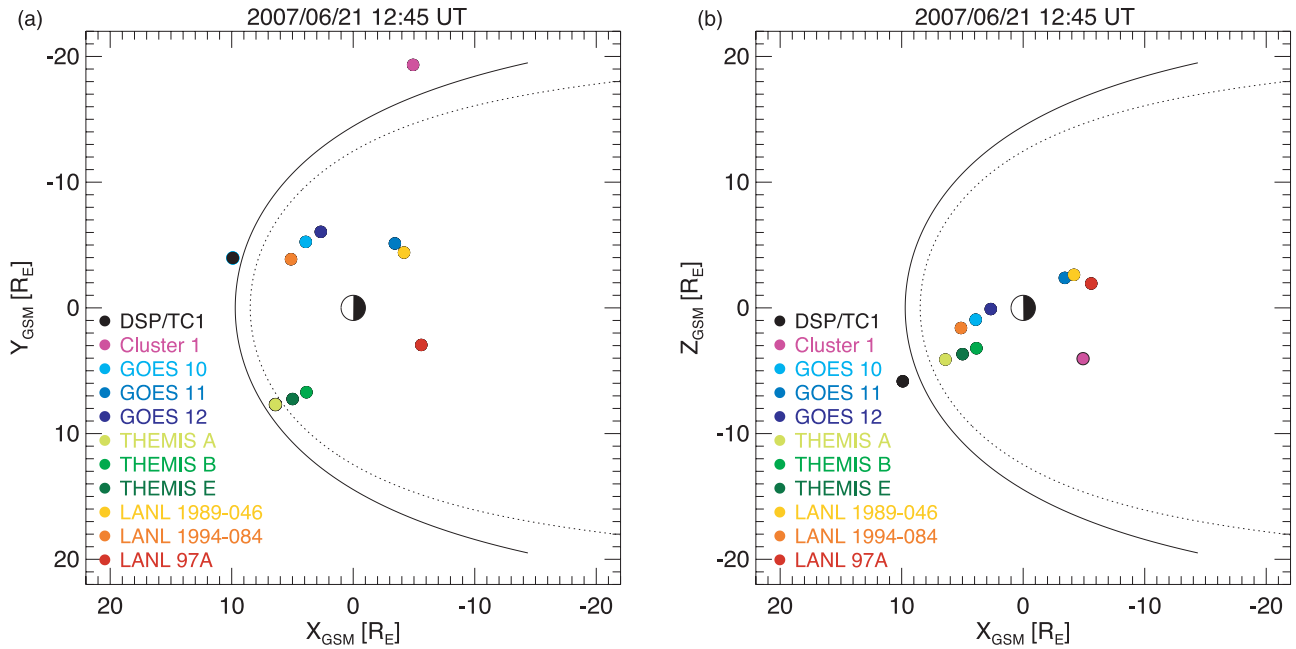
Figure 1. Spacecraft positions in GSM coordinates in the (a) *X-Y* and (b) *X-Z* planes.

the ground and Pi2 onset; they range from a few min to 20 min and peak at 9 min. Even recent studies assumed (or sometimes did not consider) the time differences and did not take into account the SI propagation inside the magnetosphere. This is partly because enough multipoint observations in the magnetosphere have not been available.

[4] On 21 June 2007, a substorm occurred <2 min after a discontinuity accompanied by a P_d increase arrived at the dayside magnetopause. In this paper, in order to investigate how this type of substorms is triggered, we estimate the propagation of the observed SIs in the magnetosphere, determine arrival time of the SI front at the plasma sheet, and compare it with substorm onset time. The estimate of the SI propagation is made with data from the GOES spacecraft and the Time History of Events and Macroscale Interactions During Substorms (THEMIS) spacecraft [*Angelopoulos*, 2008]. We also conduct 2-D calculations of the fast-mode propagation in the magnetic equatorial plane. The estimate of the substorm onset time is based on aurora brightening observed by the Polar spacecraft, dispersed electron injection observed by the Los Alamos National Laboratory (LANL) satellites, and geomagnetic negative bays at high latitudes. The comparison between the arrival time of the SI front and the substorm onset time suggests that the examined substorm expansion was triggered when the SI front reached the near-Earth plasma sheet.

2. Data Set

[5] Table 1 lists positions of the spacecraft used in the present study. Figure 1 shows the positions, except for Wind and Polar, in the *XY* and *XZ* planes in GSM coordinates. As a solar wind monitor, we use the WIND Magnetic Field Investigation (MFI) [*Lepping et al.*, 1995] and the WIND 3-D Plasma and Energetic Particle Investigation [*Lin et al.*, 1995].

[6] For solar wind observations in the magnetosheath, we use 4-s magnetic field data obtained by the Magnetic Field

Investigation (FGM) instrument onboard Double Star Programme Tan Ce 1 (DSP/TC1) [*Carr et al.*, 2005] and 4-s magnetic field data obtained by the FluxGate Magnetometer (FGM) instrument [*Balogh et al.*, 2001] and plasma moment data by the Hot Ion Analyzer (HIA) [*Rème et al.*, 2001] onboard the Cluster spacecraft.

[7] For observations in the magnetosphere, we use 0.512-s magnetic field data from the GOES 10, 11, and 12 spacecraft on the dawn side and 3-s spin-fit magnetic field data obtained by the Fluxgate Magnetometer (FGM) [*Auster et al.*, 2008] onboard THEMIS on the dusk side. The Synchronous Orbit Particle Analyzer (SOPA) [*Belian et al.*, 1992] onboard LANL measures electrons with energies of 50 keV to 26 MeV. We use 10-s electron data from three LANL satellites: 1989-046, 1994-084, and LANL-97A. The Ultraviolet Imager (UVI) [*Torr et al.*, 1995] onboard Polar provides aurora images in the far ultraviolet wavelength range (130–190 nm) every 37 s with an angular resolution of 0.036°.

[8] We use geomagnetic fields measured at College International Geophysical Observatory (CIGO, 65.1° magnetic latitude (MLAT)) and Eagle (EAG, 66.4° MLAT) in the Geophysical Institute Magnetometer Array (GIMA) in

Table 1. Spacecraft Positions at 1245 UT

	X_{GSM} (R_E)	Y_{GSM} (R_E)	Z_{GSM} (R_E)
Wind (at 1140 UT)	263.9	16.6	21.6
DSP/TC1	9.9	−4.0	−5.84
Cluster 1	−4.9	−19.3	−4.0
GOES 10	3.9	−5.3	−0.9
GOES 11	−3.4	−5.1	2.4
GOES 12	2.7	−6.0	−0.1
THEMIS A	6.4	7.7	−4.1
THEMIS B	3.9	6.7	−3.2
THEMIS E	5.0	7.3	−3.7
Polar	−5.2	−4.7	−4.1
LANL 1989-046	−4.2	−4.4	2.6
LANL 1994-084	4.8	−4.4	−1.3
LANL-97A	−5.6	3.0	1.9
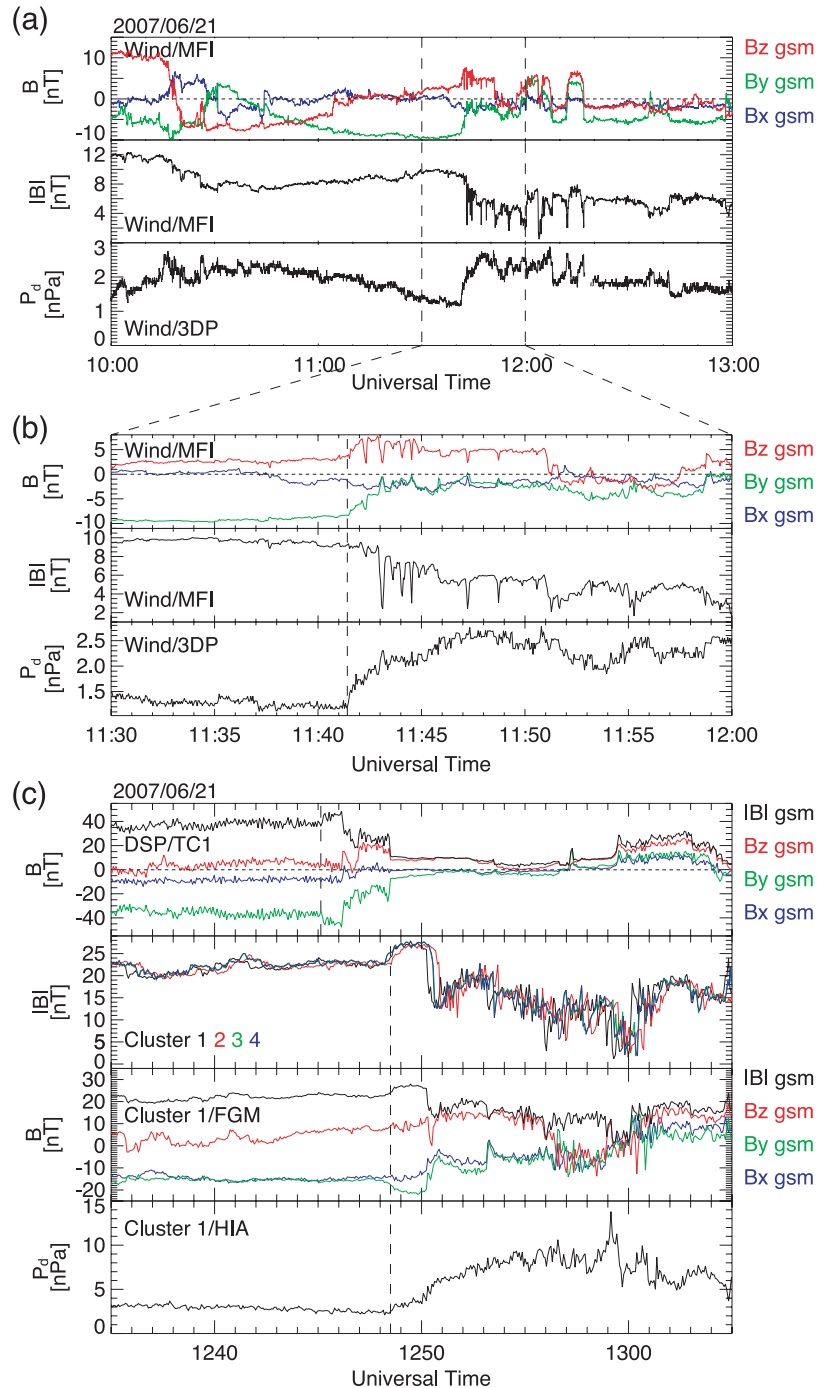
Figure 2. (a) Wind observations of the IMF and solar wind dynamic pressure between 1000 and 1300 UT. (b) A close-up of Figure 2a for 1130–1200 UT. (c) Observations in the magnetosheath by (top) DSP/TC1 and (top middle, bottom middle, and bottom) Cluster between 1235 and 1305 UT.

Alaska; and Macquarie Island (MCQ, −64.5° MLAT) in the Magnetic Data Acquisition System (MAGDAS) magnetometer chain [*Yumoto et al.*, 2006]; Fort Simpson (FSIM, 67.6° MLAT), Gillam (GILL, 66.0° MLAT), Island Lake (ISLL, 63.6° MLAT), Pinawa (PINA, 59.9° MLAT), and Rabbit Lake (RABB, 66.8° MLAT) in the Canadian Array for Real-time Investigations of Magnetic Activity (CARISMA) ground magnetometer network; and Carson City (CCNV, 45.6° MLAT), Hot Springs (HOTS, 54.3° MLAT), Pine Ridge

(PINE, 51.4° MLAT), and Prince George (PGEO, 59.3 MLAT) in the THEMIS ground-based magnetometer network [*Russell et al.*, 2008].

3. Observations

3.1. Solar Wind Observations

[9] Figure 2a shows solar wind observations by Wind between 1000 and 1300 UT. Figure 2b is a close-up for
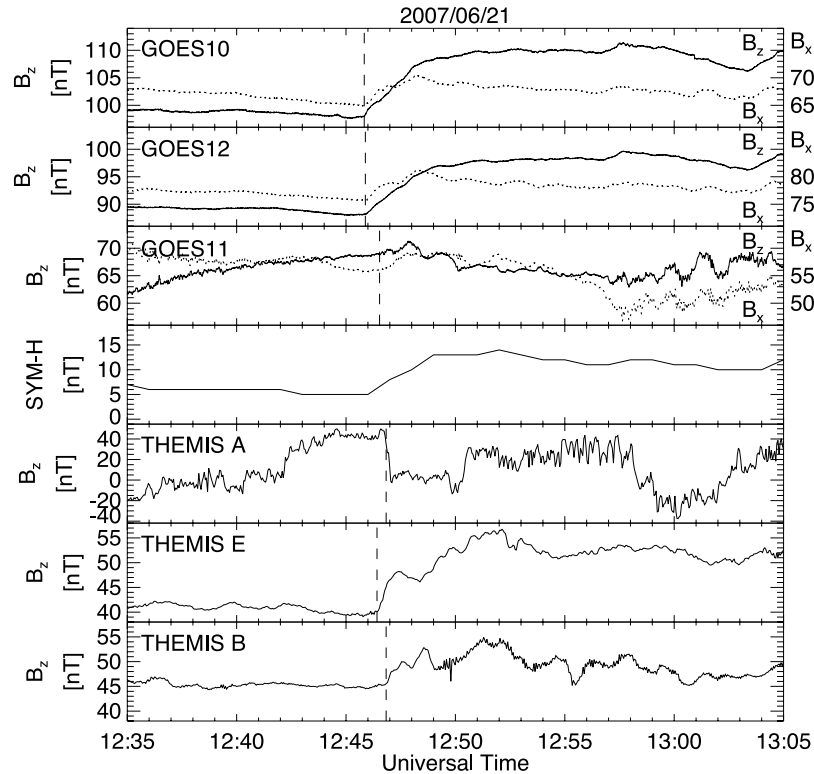
Figure 3. Magnetic field variations observed in the magnetosphere and the *SYM-H* index. All spacecraft except for THEMIS A saw sudden impulses at the times indicated by dashed lines. THEMIS A crossed the magnetopause, as indicated by a dashed line.

1130–1200 UT. Wind observed a sudden increase in P_d by a factor of ∼2 which started at 1141:20 UT. The IMF was changed simultaneously. B_y (B_z) was dominant prior to (after) the change. While B_z was positive on both sides of the change, it was negative at ∼1018–1110 UT.

[10] DSP/TC1 and Cluster observed a sudden change in the magnetic field in the magnetosheath, as shown in Figure 2c. The magnetic field observations by DSP/TC1 (Figure 2c (top)) show an increase in the magnetic field strength ($|B|$) at ∼1245:10 UT followed by its decrease to the level lower than the preincreased level at 1246–1247 UT. B_y decreased at ∼1245:10 UT, followed by its increase at 1246–1247 UT. Cluster also observed a similar structure. $|B|$ increased at ∼1248:30 UT and decreased between 1250 and 1251 UT Figure 2c (top middle). B_y at Cluster 1 shows a decrease at ∼1248:30 UT followed by an increase at 1250–1251 UT (Figure 2c (bottom middle). B_y at the other Cluster probes has a quite similar profile (not shown here). Compared with the $|B|$ and B_y observations by Wind (Figure 2b), the $|B|$ decrease and B_y increase seen at DSP/TC1 and Cluster correspond to the passage of the discontinuity. The $|B|$ increase and B_y decrease ahead of the discontinuity, on the other hand, can be seen only in the magnetosheath, is probably due to the passage of the forward fast shock generated at the bow shock through the interactions between the P_d increase discontinuity and the bow shock [*Keika et al.*, 2009]; a similar case of the interactions is reported by *Maynard et al.* [2008]. P_d at Cluster 1 increased at 1248:30 and 1250:50 UT.

3.2. Sudden Impulses in the Magnetosphere

[11] Figure 3 plots the *SYM-H* index [*Iyemori*, 1990] and magnetic field variations in the magnetosphere observed by GOES and THEMIS between 1235 and 1305 UT. GOES 10 and 12 observed SIs at 1245:50 and 1245:53 UT on the morning side, respectively, and GOES 11 detected an SI starting near 1246:30 UT at 0342 MLT. The 1-min *SYM-H* index showed a sudden increase by 8 nT within 3 min. THEMIS A on the dusk side observed a sudden decrease in B_z down to ∼0 nT at 1246:50 UT, indicating that THEMIS A crossed the magnetopause into the magnetosheath. The crossing is due to the inward motion of the magnetopause caused by a P_d increase in the fast forward shock. In fact, THEMIS A detected solar wind ions at 1247 UT and observed the discontinuity at about 1250 UT (not shown here). THEMIS E and B observed SIs starting at 1246:20 and 1246:50 UT, respectively. The profile, which is different from B_z observed by GOES, may be associated with the interactions of the solar wind discontinuity with the bow shock and/or a result of a quasi-static change of the magnetopause position, because THEMIS B and E are located only 1–2 R_E away from the magnetopause.

3.3. Substorm Activity

[12] Figure 4 includes two keograms of auroral brightening: the brightenings averaged over magnetic local time (MLT) of 21–3 h (Figure 4 (top)) and MLAT of 60–80° (Figure 4 (bottom)). Small brightening started at ∼1237 until ∼1246 UT, mainly localized at 21–22 and 0000–0130 MLT.
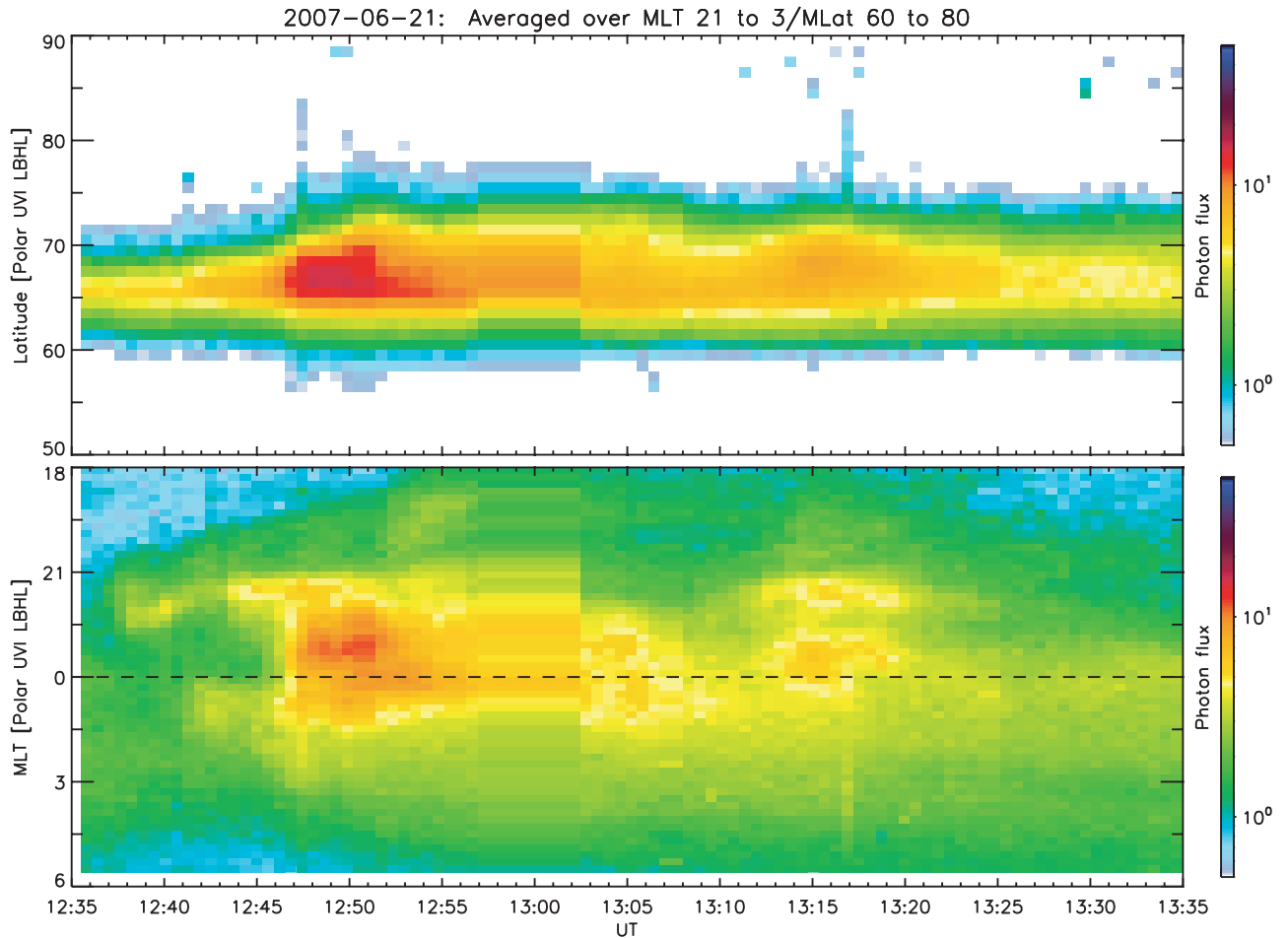
Figure 4. Keograms of auroral brightening observed by Polar/UVI in the Southern Hemisphere. The brightenings averaged over (top) magnetic latitude of $60-80°$ and (bottom) magnetic local time of $21-3$ h, respectively. An auroral brightening was suddenly intensified at $1246{:}32-1247{:}08$ UT, followed by poleward expansion.

Intense brightening occurred at $1246-1247$ UT, followed by poleward expansion which continued until $\sim$1252 UT. This major intensification was centered at $\sim$2300 MLT.

[13] Figure 5 is a sequence of auroral images in an MLT-MLAT grid from 1243:28 to 1250:49 UT. The images confirm that the major auroral intensification was centered at $\sim$2300 MLT and that two localized small brightening preceding the auroral expansion are concentrated at different local time from the major intensification. We believe that the localized brightening is not related to the substorm activity.

[14] A gradual small increase in auroral brightening can be seen in a wide range of MLT in the images for $1245{:}18-1245{:}55$ and $1245{:}55-1246{:}32$ UT. A closer look at auroral intensity during the intervals suggests that the gradual increase is a phenomenon different from the substorm, as discussed below. Figure 6 is a line plot of auroral intensity per MLT bin for different MLT sectors. Green, red, and blue lines indicate the intensity per MLT bin for $2100-2236$ (Sector A), $2236-2400$ (Sector B), and $0000-0136$ MLT (Sector C) sectors, respectively, and a black solid line shows the intensity per MLT bin for $2100-0300$ MLT. Dotted and dashed vertical lines are drawn at 1245:18 and 1246:32 UT, respectively. Auroral intensity starts increasing at the dotted line for all sectors. However, when we compare intensity increases between 1245:18 and 1246:32 UT (Interval X: between dashed and dotted lines) and between 1246:32 and 1248:22 UT (Interval Y: after the dashed line), we can see a clear difference in the increase rate. The intensity shows similar gradual increases for all three sectors for Interval X, while for Interval Y an increase in Sector B is much larger than that in Sector A and C. The dominant part of the major intensification is seen only in Sector B. The increase rate is 1.2 ($\sim$73/63), 1.8 ($\sim$58/33), and 1.4 ($\sim$69/51) for Sector A, B, and C, respectively, for Interval X. It is 1.4 ($\sim$100/73), 2.8 ($\sim$162/58), and 1.5 ($\sim$100/69) for Sector A, B, and C, respectively, for Interval Y. The time profiles of auroral intensity suggest that the gradual increase in Interval X is not related to substorm-associated auroral intensification in Interval Y. If the gradual increase in Interval X was due to the triggered substorm to be expanded, the auroral intensity in Interval Y would increase at all or at least two sectors by similar rates. Therefore we conclude that the gradual intensity increase is a phenomenon different from the substorm-related brightening. The gradual intensity increase is probably associated with the magnetospheric compression, because the increase occurred in a wide range of MLT (Sectors A, B,
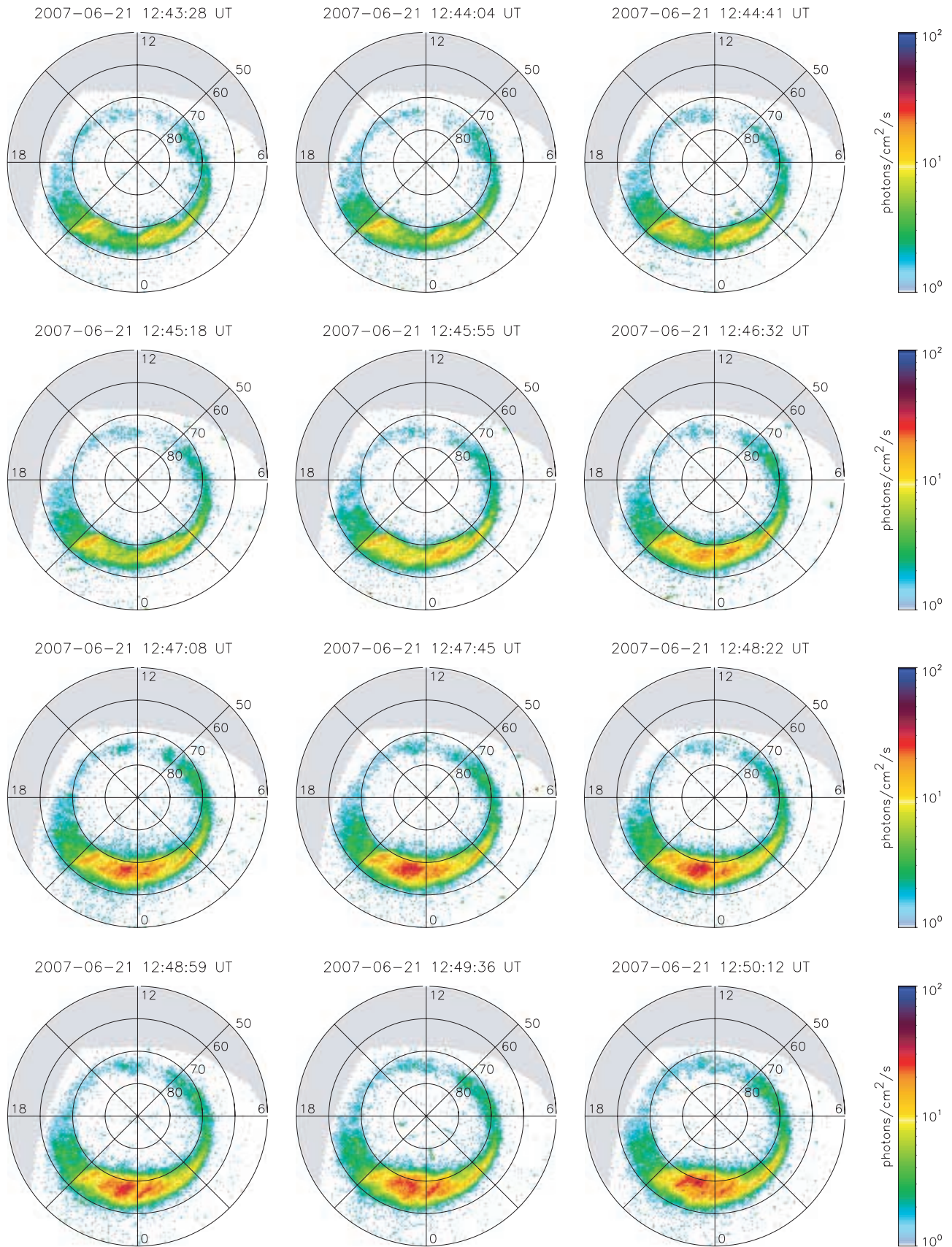
Figure 5. A sequence of aurora images obtained by Polar/UVI in the Southern Hemisphere from 1243:28 to 1250:39 UT. Each image is presented in an MLT-MLAT grid with 0000 MLT at the bottom, 0600 MLT to the right, 1200 MLT at the top, and 1800 MLT to the left.
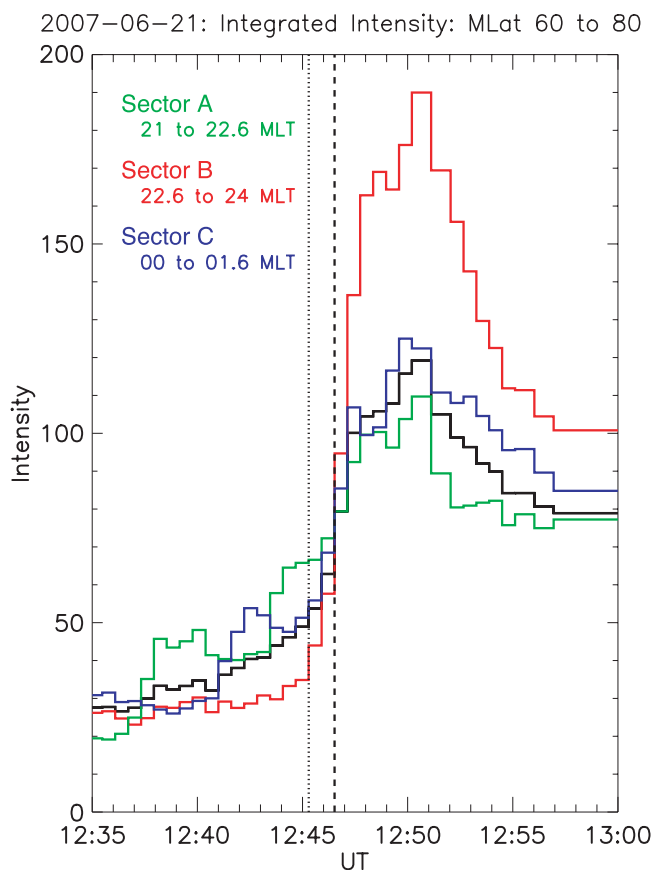
Figure 6. Auroral intensity per MLT bin for the 2100–2236 (Sector A), 2236–2400 (Sector B), and 0000–0136 MLT (Sector C) sectors, respectively. The black solid line shows the intensity for 2100–0300 MLT. Dotted and dashed vertical lines are drawn at 1245:18 and 1246:32 UT, respectively.

and C). Geomagnetic field variations at high and middle latitudes support this interpretation, as discussed below.

[15] Figure 7 shows the horizontal component of the ground magnetic field at high and middle latitudes on the dawn side. Dotted and dashed vertical lines are drawn at 1245:18 and 1246:32 UT, respectively, as in Figure 6. At high-latitude stations such as RABB, GILL, and ISLL, clear wave forms starting with positive pulses at about 1246 UT are seen. The positive pulses are followed by negative pulses, being consistent with the *DP* field of a model of the magnetospheric response to a sudden increase of the solar wind dynamic pressure [*Araki*, 1994]. In the model, the *DP* field, caused by induced field-aligned currents and iono-spheric currents, consists of positive-negative pulses in the high-latitude geomagnetic field on the morning side and negative-positive pulses on the evening side. A middle-latitude station, CCNV, saw a stepwise increase starting at about 1246 UT. The increase is consistent with the *DL* field of the model by *Araki* [1994]. The *DL* field corresponds to magnetic field disturbances caused by enhanced magneto-pause currents. At PINE and HOTS, 5–10° higher in lat-itudes, a gradual increase with pulsations can be seen. This is likely explained by a superposition of the *DL* and *DP* fields (i.e., a stepwise increase seen at middle-low latitudes and a

negative excursion with pulsations seen at high latitudes). The onset time of the clearly visible effects of the magneto-spheric compression is difficult to be identified, because small field fluctuations exist prior to 1246 UT since 1243 UT or earlier. However, we can say that the onset occurred between 1245:18 and 1246:32 UT. This supports the idea that the gradual increase in auroral intensity at 1245:18–1246:32 UT is associated with the magnetospheric compression.

[16] Figure 8a plots energetic electron flux observed by SOPA onboard LANL 1989-046 and 1994-084. Both space-craft saw dispersed electron injection; it is more dispersed at 1994-084 located at 0936 MLT than at 1989-046 at 0248 MLT. LANL 97A did not see clear electron injections at ~2206 MLT (not shown here). We estimate onset UT and MLT of the injection, assuming that the dispersion results from the azimuthal gradient B drift under a constant magnetic field. Since the speed of the gradient B drift is proportional to the energy of the electrons, the inverse of the energy ($1/W$) is proportional to the time required for the injected electrons to reach a spacecraft position. Figure 8b shows $1/W$ as a function of time for an injection local onset and a flux peak at LANL/ 1989-046 and a flux peak at LANL/1994-084. The dashed lines present regression lines determined by least squares fits. We estimate the injection onset UT to be 1248:20 UT, taking the intersection between the $1/W = 0$ line and the regression line for the local onset at LANL/1989-046. We also estimate the azimuthal drift speed to be 0.23 MLT/h/keV on average,
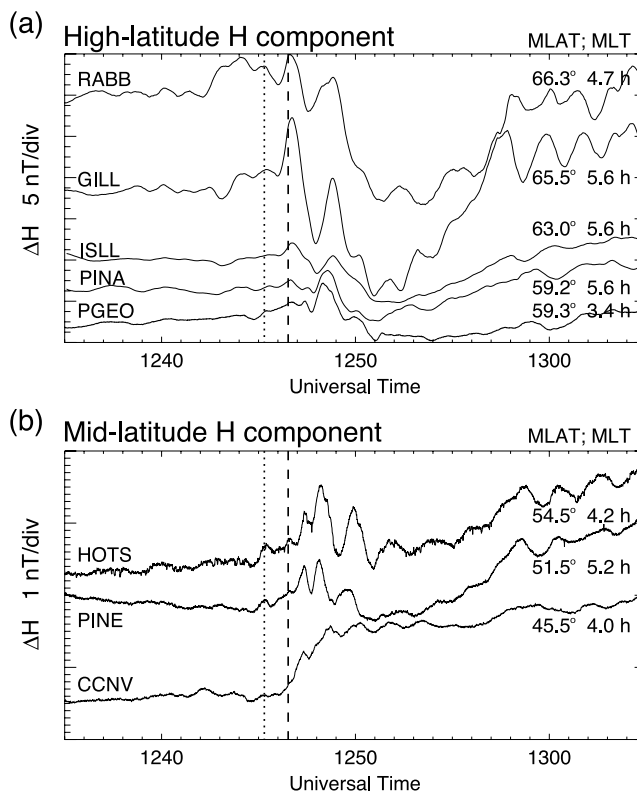
Figure 7. Geomagnetic field horizontal component at (a) high and (b) middle latitudes. Dotted and dashed vertical lines are drawn at 1245:18 and 1246:32 UT, respectively. The numbers on the right-hand side present magnetic latitude and magnetic local time at 1245 UT.
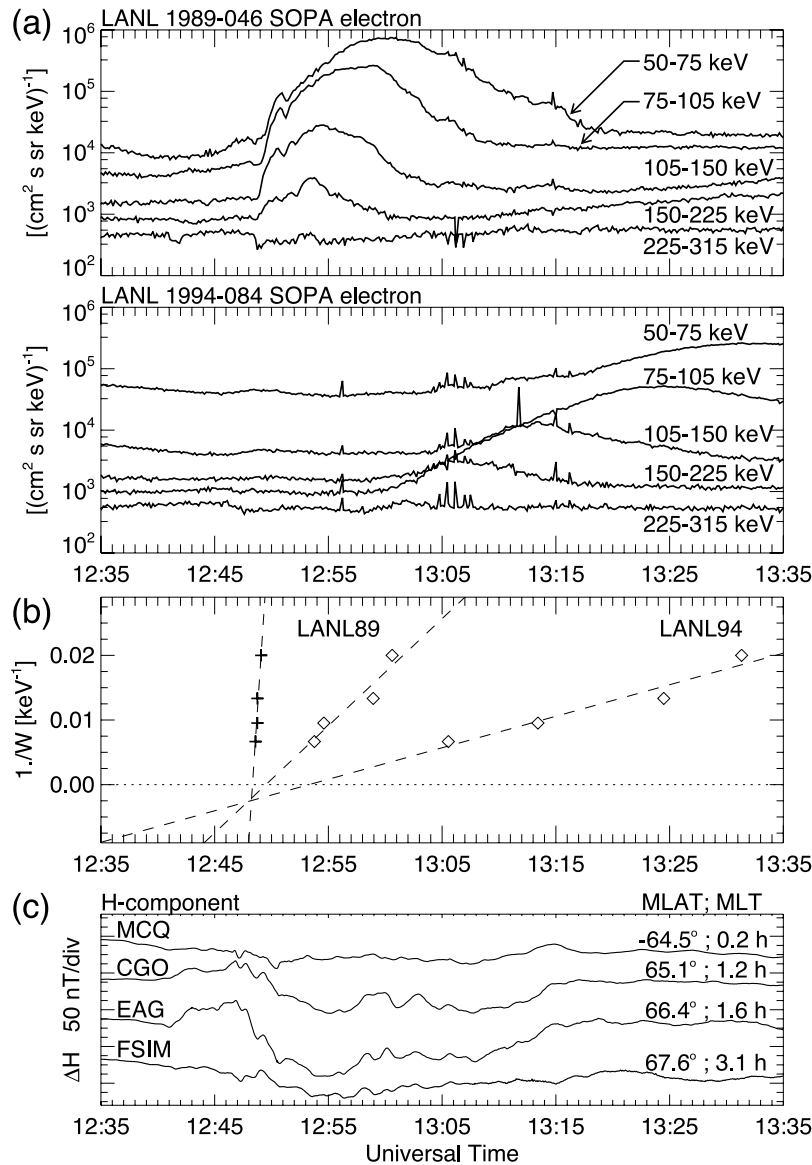
Figure 8. (a) Energetic electron flux observed by LANL/SOPA. Spacecraft 1989-046 and 1994-084 were located at 0248 and 0936 MLT, respectively. (b) The inverse of electron energy as a function of time. Plus signs correspond to the local injection onset at 1989-046, and diamonds correspond to injection peaks at both spacecraft. Dashed lines are regression lines determined by the least squares fit. (c) High-latitude geomagnetic field variations. The numbers on the right-hand side present magnetic latitude and magnetic local time at 1248 UT.

using the times of flux peaks for each energy range. The estimated onset UT and drift speed give onset MLT, which is calculated to be 0112 MLT on average.

[17] Figure 8c shows the geomagnetic field variations from high-latitude night side stations between 1235 and 1335 UT. Negative bays in the H component of the geomagnetic field are observed in auroral regions. They started near 1248 UT and the amplitude was maximized at 0136 MLT.

[18] We see a discrepancy in the substorm onset MLT between auroral images and our estimates from electron injections. We attribute the discrepancy to the B_y-dominant IMF. The IMF was directed northward and dawnward before the discontinuity impinged on the magnetosphere, dominated by the dawnward component: $B_y \sim -8$ nT and $B_z \sim 3$ nT. Statistics of auroral features seen by global imaging in the conjugate hemisphere [Østgaard et al., 2005, 2007] showed dawn-dusk displacement of auroral onset locations. An auroral onset in the Southern Hemisphere is located dawnward of that in the Northern Hemisphere when IMF clock angle is $270° \pm 60°$, where the clock angle is defined as the counterclockwise angle around the X axis with respect to the northward direction. For the examined event, since the clock angle is $\sim 280°$, the relative displacement would have occurred. We believe that the electrons injected around 0100–0200 MLT precipitated into the Southern Hemisphere at ~ 2300 MLT along the twisted field line.
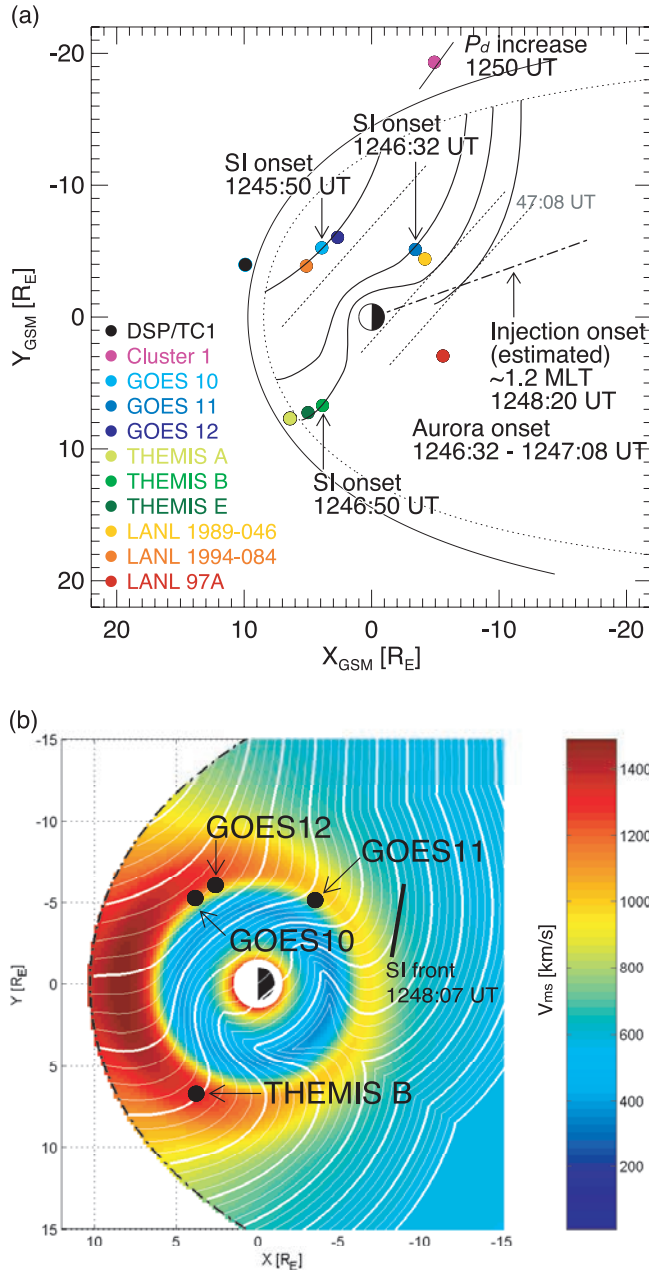
Figure 9. (a) Summary of the observations and illustration of the SI propagation. Dotted lines represent the estimated SI front. Solid curved lines illustrate the deformed SI front; changes in fast-mode speed are taken into account. The dashed-dotted line is drawn at the estimated MLT of the substorm expansion onset. The magnetopause (MP) is based on *Shue et al.*'s [1998] model. We chose parameters for the model so that it can explain the MP crossing of THEMIS A; the solid and dotted lines correspond to MP before and after the magnetospheric compression. (b) Results of 2-D calculations of the fast-mode propagation in the magnetic equatorial plane with the source front that is 45° inclined toward dusk. Positions of GOES 10, 11, and 12 and THEMIS B are embedded. Color contours show fast-mode speeds. White curve lines are the calculated wavefront, drawn every 5 s with thick lines every 20 s. The solid straight line indicates the SI front at the time corresponding to 1248:07 UT.

3.4. SI Propagation and Substorm Onset

3.4.1. Observations

[19] The multipoint observations of the SIs on the dawn and dusk sides enable us to estimate the propagation speed and normal of the SI front. Using three spacecraft on the dayside, GOES 10, GOES 12, and THEMIS B, we estimated the speed and normal in the *X-Y* plane in GSM coordinates to be $\varphi = 138°$ and 850 km/s, where φ is the longitude in GSM coordinates. Using these values, we estimate the front arrival time at GOES 11 under the assumption that the normal and speed are constant throughout the propagation toward the magnetotail. The estimated arrival time is 1246:32 UT, which is almost consistent with the time of the SI observation by GOES 11, although it is difficult to accurately determine its onset time on the second time scale.

[20] Figure 9a summarizes the estimate along with the observations addressed in section 3.2 and the estimates of the auroral expansion and injection onset time shown in section 3.3. Dotted straight lines represent the SI front estimated from the observations on the dayside. Solid curved lines are illustrations of the SI front propagation; a decrease in the fast-mode velocity in the plasmasphere is taken into account. The dashed-dotted line represents the electron injection onset MLT estimated in section 3.3. The SI front generated at the dayside magnetopause was at GOES 11 at 1246:32 UT, while it can reach the dawnside plasma sheet, $(X, Y) \sim (-9, -5) R_E$, at 1247:08 UT, if we assume the front normal and speed are constant.

3.4.2. Calculations

[21] We examine the propagation of the SIs with the help of 2-D calculations of the fast-mode propagation in the magnetic equatorial plane. The calculation algorithm is developed by *Chi et al.* [2007]. The wavefront movement of the propagation follows the Huygens' principle. The algorithm allows us to define the shape of the initial wavefront and track the wavefront movement in the equatorial plane. The duration of each time step is 1 s. We focus on the fast-mode speed in the magnetosphere on the basis of the following quantities. For the magnetic field, we use a model by *Tsyganenko* [1989] and a magnetopause model by *Shue et al.* [1998]. For the mass density, we use: n [kg cm^{-3}] $= 200 \times (5/r)^4 m$ for the plasmasphere, n [kg cm^{-3}] $= 0.6 \times (10/r)^4 m$ for the plasmatrough, and n [kg cm^{-3}] $= 0.6/(1 - \exp(-r/12))m$ for the plasma sheet, where r is the radial distance in R_E and m is proton mass; and the plasmapause is set at 5.52 R_E, as estimated by the empirical model of *Carpenter and Anderson* [1992]. The temperature is $(2000 - 1000 \cos \varphi)/(1 - 0.5 \exp(-r/12))$ eV, where φ is the angle from the direction of local noon. The density and temperature between two connecting regions are smoothed by a *tanh* function.

[22] Figure 9b displays results of the 2-D calculations initiated with the source wavefront that is 45° inclined toward dusk. Color contours represent fast-mode speeds. The white curve lines are the estimated wavefront; the lines are drawn every 5 s and thick lines every 20 s. Positions of GOES 10, 11, and 12 and THEMIS B are embedded in Figure 9b. The calculations are successful in explaining earlier arrival at GOES 11 than at THEMIS B. The mean propagation speed is calculated to be 903 km/s from GOES 12 to GOES 11, being in a good agreement with that estimated from the multipoint observations of the SIs. Aurora expansion onset identified by the Polar/UVI observations (see section 3.3) was 0−37 s

later than the SI observation by GOES 11. The calculated wavefront can reach the dawnside near-Earth plasma sheet at $(X, Y) \sim (-9, -5)\ R_E$ by the time of auroral expansion onset, as indicated by the solid line.

4. Discussion

[23] We examined a substorm expansion on 21 June 2007, which occurred <2 min after a solar wind discontinuity accompanied by a P_d increase arrived at the dayside magnetopause. We used a large number of in situ observations of SIs, a set of auroral imaging, and geomagnetic field measurements. The multipoint observations enabled us to estimate arrival time of the SI front at the plasma sheet and compare it with onset time of the substorm expansion. We calculated propagation speed and normal of the SI front to be $\varphi = 138°$ and 850 km/s. We estimated onset MLT to be $1.2-1.6$ h from the observations of dispersed electron injection and negative bays of the geomagnetic field. This indicates that the substorm expansion onset occurred in the dawnside plasma sheet. Auroral images showed the auroral expansion starting at a window of $1246:32-1247:08$ UT. The SI front can reach the dawnside plasma sheet, $(X, Y) \sim (-9, -5)\ R_E$ at the auroral expansion onset, if we assume that the front normal and speed are constant. Although the speed becomes slow in the plasmasphere because of a decrease in the Alfvén speed due to the higher density and therefore the SI front is deformed, the assumption is valid enough for the following two reasons. The SI observations used in this study were made outside of the plasmasphere. The averaged normal propagation speed derived from our 2-D calculations of the fast-mode propagation was in good agreement: 902 km/s. In the calculations, the SI front can reach the dawnside plasma sheet at the time corresponding to 1247:08 UT. Thus, we conclude that the substorm expansion was triggered by the arrival of the SI front propagating from the dayside magnetopause.

[24] We propose that the inductive dawnward electric field on the SI front is a possible candidate to trigger the substorm expansion examined in the present study. When a solar wind discontinuity suddenly compresses the dayside magnetosphere, the dawnward electric field is induced on the SI front [cf., *Araki*, 1994]. Such an inductive electric field was detected in the plasma sheet by Cluster located at $X = -19\ R_E$ at the time of magnetospheric compression on 24 August 2005 [*Keika et al.*, 2008]. Although detailed physical processes remain unrevealed, our suggestion is reasonable at least qualitatively because the sudden increase of the dawnward electric field in the plasma sheet has the same characteristics as a reduction in the duskward convection electric field at the time of a northward turning of the IMF which has been believed to be one of the major triggers [e.g., *Lyons et al.*, 2003]. The inductive dawnward electric field, which is related to dynamic motion of the dayside magnetopause, could be one of the important fields to substorm triggering.

[25] The present analysis has only considered propagation in the magnetic equatorial plane through the plasma sheet. An SI front, however, can propagate faster in the lobe than in the plasma sheet, because the fast-mode speed is faster in the lobe than in the plasma sheet. In fact, *Sugiura et al.* [1968] demonstrated that the SI front on 8 July 1966, which was estimated to be 20° inclined toward dusk, took $1.5-2$ min to reach OGO-3 located in the lobe on the dusk side at $(X, Y, Z)_{GSM} = (-10.10, 10.27, 11.55)\ R_E$ from the dayside magnetopause. The SI front of the present event could have passed through the near-Earth plasma sheet earlier and arrived further tailward at the substorm expansion onset. These characteristics support our conclusions qualitatively.

[26] A large number of studies have examined and discussed substorm triggering by compression of the whole magnetotail [e.g., *Lyons et al.*, 2005; *Hubert et al.*, 2006]. The lateral compression of the magnetotail is one of the probable candidates to trigger substorms. Several studies have reported that disturbances associated with the lateral compression characterize the SIs in the lobe [*Kawano et al.*, 1992; *Collier et al.*, 1998; *Kim et al.*, 2004; *Huttunen et al.*, 2005]. The substorm expansion examined in the present study was, however, not triggered by the lateral compression. Cluster in the dawnside magnetosheath at $X \sim -5\ R_E$ observed a P_d increase at 1248:30 UT or later. This strongly suggests that the magnetotail was not yet compressed at the substorm expansion onset (earlier than 1248 UT). In addition, the Open Geospace General Circulation Model (OpenGGCM) demonstrated that the magnetic field in the lobe adjacent to the plasma sheet increases about 10 min after the solar wind discontinuity impinges on the dayside magnetopause (not shown here).

[27] Whether a substorm is triggered by the magnetospheric compression or not has been believed to depend on preconditions in the magnetotail, in particular in the plasma sheet, as discussed in the studies using global aurora images [e.g., *Lyons et al.*, 2005; *Meurant et al.*, 2005]. For the present event, the plasma sheet could have been in a preferable condition to the triggering of the substorm expansion. In fact, from Wind observations shown in Figure 2a, IMF B_z was negative for about 50 min until $\sim$1110 UT (until $\sim$30 min prior to the arrival of the discontinuity for both cases) and dominated at $\sim$1030$-\sim$1050 UT.

[28] Wind observations showed a decrease in the magnitude of B_y ($|B_y|$) associated with the P_d increase across the discontinuity (see Figure 2b). The $|B_y|$ decrease has a potential to reduce the convection electric field in the magnetosphere. However, for the present event, the $|B_y|$ decrease is unlikely to be responsible for the electric field reduction and the substorm triggering. We explain our interpretations in detail below.

[29] The magnetic field at DSP/TC1 in the dayside magnetosheath (Figure 2c (top)) shows that $|B_y|$ increases at 1245:10 UT and decreases at 1246:10 UT. The increase is probably related to the fast shock generated at the bow shock through interactions between the discontinuity and the bow shock, and the decrease took place at the discontinuity [*Keika et al.*, 2009]. Cluster 1 observations (Figure 2c (bottom middle and bottom)) show similar profiles of the magnetic field and an increase in dynamic pressure at both the fast shock ($\sim$1248 UT) and the discontinuity ($\sim$1250 UT). The observations suggest that the dynamic pressure increases at both 1245:10 and 1246:10 UT at DSP/TC1. GOES 10 and 12 in the dayside magnetosphere saw the SI onset at 1245:50 and 1245:53 UT, respectively. The SI onset took place after the fast shock arrived at DSP/TC1 and before the discontinuity reached DSP/TC1. Therefore, the SI onset results from the impact of the fast shock which involves a $|B_y|$ increase. A MHD simulation by *Maynard et al.* [2008]

has showed the initiation of the magnetopause motion determined by the arrival of the fast shock generated through interactions between a pressure increase discontinuity and the bow shock.

[30] The $|B_y|$ decrease across the discontinuity is considered to reach the dayside magnetopause soon after 1246:10 UT. The auroral onset time was within an observation bin of 1246:32−1247:08 UT. We believe that the effect of the $|B_y|$ decrease is difficult to reach the magnetotail within 1 min. Even the fast-mode propagation takes 1.5−2 min. Furthermore, a change in the global magnetotail configuration due to the $|B_y|$ decrease is sure to take much longer, because the $|B_y|$ decrease should be convected at a solar wind speed and in fact reached Cluster at X ∼ −5 R_E at as late as ∼1250 UT, ∼3 min after the auroral onset. From a viewpoint of timing analysis shown above, we conclude that the $|B_y|$ decrease is unlikely a trigger of the examined substorm.

5. Summary and Conclusions

[31] We examined the substorm expansion triggered <2 min after the time when a solar wind discontinuity accompanied by a P_d increase impinged on the dayside magnetopause, using multipoint observations of SIs and substorm activity. GOES 10 and 12 on the dawn side and THEMIS B on the dusk side observed SIs at 1245:50, 1245:53, and 1246:50 UT, respectively. GOES 11 on the dawn side at night observed an SI near 1246:30 UT, 20 s earlier than THEMIS B in the dayside magnetosphere. The SI front was 42° inclined toward dusk, propagating with the speed of 850 km/s. Aurora expansion onset was in a window of 1246:32−1247:08 UT, followed by poleward and azimuthal expansion. LANL 1989-046 at ∼0248 MLT and 1994-084 at ∼0936 MLT saw dispersed electron injection. The analysis of the dispersed injection showed that injection onset MLT was ∼0112 MLT. The geomagnetic field data obtained at high latitudes on the night side show negative bays in the H component, which were maximized near 0136 MLT. Our estimates and 2-D calculations demonstrated that the SI front can reach the substorm expansion onset site (i.e., dawnside near-Earth plasma sheet) at the onset time. The magnetotail was not yet compressed at the onset time. We suggest that the substorm expansion was triggered by the arrival of the SI front propagating from the dayside magnetopause, and not triggered by the disturbances generated by the motion of the flank magnetopause. The inductive dawnward electric field on the SI front is a possible trigger of the substorm.

References

Angelopoulos, V. (2008), The THEMIS mission, *Space Sci. Rev.*, *141*, 5–34, doi:10.1007/s11214-008-9336-1.

Araki, T. (1994), A physical model of the geomagnetic sudden commencement, in *Solar Wind Sources of Magnetospheric Ultra-Low-Frequency Waves*, vol. 81, edited by M. J. Engebretson, K. Takahashi, and M. Scholer, pp. 183–200, AGU, Washington, D. C.

Aubry, M. P., and R. L. McPherron (1971), Magnetotail changes in relation to the solar wind magnetic field and magnetospheric substorms, *J. Geophys. Res.*, *76*, 4381–4401, doi:10.1029/JA076i019p04381.

Auster, H. U., et al. (2008), The THEMIS fluxgate magnetometer, *Space Sci. Rev.*, *141*, 235–264, doi:10.1007/s11214-008-9365-9.

Balogh, A., et al. (2001), The Cluster magnetic field investigation: Overview of in-flight performance and initial results, *Ann. Geophys.*, *19*, 1207–1217.

Belian, R. D., G. R. Gisler, T. Cayton, and R. Christensen (1992), High-z energetic particles at geostationary orbit during the great solar proton event series of October 1989, *J. Geophys. Res.*, *97*, 16,897–16,906, doi:10.1029/92JA01139.

Burch, J. L. (1972), Preconditions for the triggering of polar magnetic substorms by storm sudden commencements, *J. Geophys. Res.*, *77*, 5629–5632, doi:10.1029/JA077i028p05629.

Carpenter, D. L., and R. R. Anderson (1992), An ISEE/whistler model of equatorial electron-density in the magnetosphere, *J. Geophys. Res.*, *97*, 1097–1108, doi:10.1029/91JA01548.

Carr, C., et al. (2005), The Double Star magnetic field investigation: Instrument design, performance and highlights of the first year's observations, *Ann. Geophys.*, *23*, 2713–2732.

Chi, P. J., C. T. Russell, and V. Angelopoulos (2007), Travel time of impulsive signals in the magnetosphere: Modeling and observations, *Eos Trans. AGU*, *88*(52), Fall Meet. Suppl., Abstract SM11A-0314.

Collier, M. R., J. A. Slavin, R. P. Lepping, K. Ogilvie, A. Szabo, H. Laakso, and S. Taguchi (1998), Multispacecraft observations of sudden impulses in the magnetotail caused by solar wind pressure discontinuities: Wind and IMP8, *J. Geophys. Res.*, *103*, 17,293–17,305, doi:10.1029/97JA02870.

Foster, J. C., D. H. Fairfield, K. W. Ogilvie, and T. J. Rosenberg (1971), Relationship of interplanetary parameters and occurrence of magnetospheric substorms, *J. Geophys. Res.*, *76*, 6971–6975, doi:10.1029/JA076i028p06971.

Henderson, M. G., G. D. Reeves, R. D. Belian, and J. S. Murphree (1996), Observation of magnetospheric substorms occurring with no apparent solar wind/IMF trigger, *J. Geophys. Res.*, *101*, 10,773–10,791, doi:10.1029/96JA00186.

Horwitz, J. L. (1985), The substorm as an internal magnetospheric instability: Substorms and their characteristic time scales during intervals of steady interplanetary magnetic field, *J. Geophys. Res.*, *90*, 4164–4170, doi:10.1029/JA090iA05p04164.

Hubert, B., M. Palmroth, T. V. Laitinen, P. Janhunen, S. E. Milan, A. Grocott, S. W. H. Cowley, T. Pulkkinen, and J. C. Gérard (2006), Compression of the Earth's magnetotail by interplanetary shocks directly drives transient magnetic flux closure, *Geophys. Res. Lett.*, *33*, L10105, doi:10.1029/2006GL026008.

Huttunen, K. E. J., J. Slavin, M. Collier, H. E. J. Koskinen, A. Szabo, E. Tanskanen, A. Balogh, E. Lucek, and H. R. Rème (2005), Cluster observations of sudden impulses in the magnetotail caused by interplanetary shocks and pressure increases, *Ann. Geophys.*, *23*, 609–624.

Iyemori, T. (1990), Storm-time magnetospheric currents inferred from mid-latitude geomagnetic field variations, *J. Geomag. Geoelectr.*, *42*, 1249–1265.

Iyemori, T., and S. Tsunomura (1983), Characteristics of the association between an sc and a substorm onset, *Mem. Natl. Inst. Polar Res. Spec. Issue Jpn.*, *26*, 139–148.

Kawano, H., T. Yamamoto, S. Kokubun, and R. P. Lepping (1992), Rotational polarities of sudden impulses in the magnetotail lobe, *J. Geophys. Res.*, *97*, 17,177–17,182, doi:10.1029/92JA01250.

Keika, K., et al. (2008), Response of the inner magnetosphere and the plasma sheet to a sudden impulse, *J. Geophys. Res.*, *113*, A07S35, doi:10.1029/2007JA012763.

Keika, K., et al. (2009), Deformation and evolution of solar wind discontinuities through their interactions with the Earth's bow shock, *J. Geophys. Res.*, doi:10.1029/2008JA013481, in press.

Kim, K. H., C. A. Cattell, D. H. Lee, A. Balogh, E. Lucek, M. Andre, Y. Khotyaintsev, and H. Rème (2004), Cluster observations in the magnetotail during sudden and quasiperiodic solar wind variations, *J. Geophys. Res.*, *109*, A04219, doi:10.1029/2003JA010328.

Kokubun, S., R. L. McPherron, and C. T. Russell (1977), Triggering of substorms by solar wind discontinuities, *J. Geophys. Res.*, *82*, 74–86, doi:10.1029/JA082i001p00074.

Lepping, R. P., et al. (1995), The Wind magnetic-field investigation, *Space Sci. Rev.*, *71*, 207–229, doi:10.1007/BF00751330.

Lin, R. P., et al. (1995), A three-dimensional plasma and energetic particle investigation for the Wind spacecraft, *Space Sci. Rev.*, *71*, 125–153, doi:10.1007/BF00751328.

Liou, K., P. T. Newell, C. I. Meng, C. C. Wu, and R. P. Lepping (2003), Investigation of external triggering of substorms with Polar ultraviolet imager observations, *J. Geophys. Res.*, *108*(A10), 1364, doi:10.1029/2003JA009984.

Lyons, L. R. (1996), Substorms: Fundamental observational features, distinction from other disturbances, and external triggering, *J. Geophys. Res.*, *101*, 13,011–13,025, doi:10.1029/95JA01987.

Lyons, L. R., S. Liu, J. M. Ruohoniemi, S. I. Solovyev, and J. C. Samson (2003), Observations of dayside convection reduction leading to substorm onset, *J. Geophys. Res.*, *108*(A3), 1119, doi:10.1029/2002JA009670.

Lyons, L. R., D. Y. Lee, C. P. Wang, and S. B. Mende (2005), Global auroral responses to abrupt solar wind changes: Dynamic pressure, substorm, and null events, *J. Geophys. Res.*, *110*, A08208, doi:10.1029/2005JA011089.

Maynard, N. C., C. J. Farrugia, D. M. Ober, W. J. Burke, M. Dunlop, F. S. Mozer, H. Rème, P. Décréau, and K. D. Siebert (2008), Cluster observations of fast shocks in the magnetosheath launched as a tangential discontinuity with a pressure increase crossed the bow shock, *J. Geophys. Res.*, *113*, A10212, doi:10.1029/2008JA013121.

McPherron, R. L., T. Terasawa, and A. Nishida (1986), Solar wind triggering of substorm expansion onset, *J. Geomag. Geoelectr.*, *38*, 1089–1108.

Meurant, M., J. C. Gerard, C. Blockx, V. Coumans, B. Hubert, M. Connors, L. R. Lyons, and E. Donovan (2005), Comparison of intense nightside shock-induced precipitation and substorm activity, *J. Geophys. Res.*, *110*, A07228, doi:10.1029/2004JA010916.

Nishida, A. (1978), *Geomagnetic Diagnosis of the Magnetosphere*, Springer, New York.

Østgaard, N., N. A. Tsyganenko, S. B. Mende, H. U. Frey, T. J. Immel, M. Fillingim, L. A. Frank, and J. B. Sigwarth (2005), Observations and model predictions of substorm auroral asymmetries in the conjugate hemispheres, *Geophys. Res. Lett.*, *32*, L05111, doi:10.1029/2004GL022166.

Østgaard, N., S. B. Mende, H. U. Frey, J. B. Sigwarth, A. Asnes, and J. M. Weygand (2007), Auroral conjugacy studies based on global imaging, *J. Atmos. Sol. Terr. Phys.*, *69*, 249–255, doi:10.1016/j.jastp.2006.05.026.

Pellinen, R. J., W. Baumjohann, W. J. Heikkila, V. A. Sergeev, A. G. Yahnin, G. Marklund, and A. O. Melnikov (1982), Event study on presubstorm phases and their relation to the energy coupling between solarwind and magnetosphere, *Planet. Space Sci.*, *30*, 371–388, doi:10.1016/0032-0633(82)90043-5.

Rème, H., et al. (2001), First multispacecraft ion measurements in and near the Earth's magnetosphere with the identical Cluster ion spectrometry (CIS) experiment, *Ann. Geophys.*, *19*, 1303–1354.

Rostoker, G. (1983), Triggering of the expansive phase intensifications of magnetospheric substorms by northward turnings of the interplanetary magnetic field, *J. Geophys. Res.*, *88*, 6981–6993, doi:10.1029/JA088iA09p06981.

Russell, C. T., P. J. Chi, D. J. Dearborn, Y. S. Ge, B. Kuo-Tiong, J. D. Means, D. R. Pierce, K. M. Rowe, and R. C. Snare (2008), THEMIS ground-based magnetometers, *Space Sci. Rev.*, *141*, 381–412, doi:10.1007/s11214-11008-19337-11210.

Shue, J. H., et al. (1998), Magnetopause location under extreme solar wind conditions, *J. Geophys. Res.*, *103*, 17,691–17,700, doi:10.1029/98JA01103.

Sugiura, M., T. L. Skillman, B. G. Ledley, and J. P. Heppner (1968), Propagation of the sudden commencement of July 8, 1966, to the magnetotail, *J. Geophys. Res.*, *73*, 6699–6709, doi:10.1029/JA073i021p06699.

Torr, M. R., et al. (1995), A far-ultraviolet imager for the international solar-terrestrial physics mission, *Space Sci. Rev.*, *71*, 329–383, doi:10.1007/BF00751335.

Tsyganenko, N. A. (1989), A magnetospheric magnetic field model with a warped tail current sheet, *Planet. Space Sci.*, *37*, 5–20, doi:10.1016/0032-0633(89)90066-4.

Yumoto, K., et al. (2006), MAGDAS project and its application for space weather, in *Solar Influence on the Heliosphere and Earth's Environment: Recent Progress and Prospects*, edited by N. Gopalswamy and A. Bhattacharyya, pp. 309–405, Quest Publ., Mumbai, India.

Zhou, X. Y., and B. T. Tsurutani (2001), Interplanetary shock triggering of nightside geomagnetic activity: Substorms, pseudobreakups, and quiescent events, *J. Geophys. Res.*, *106*, 18,957–18,967, doi:10.1029/2000JA003028.

————————————
V. Angelopoulos and P. J. Chi, Institute of Geophysics and Planetary Physics, University of California, 3845 Slichter Hall, 603 Charles E. Young Drive E, Los Angeles, CA 90095-1567, USA.

H. U. Auster, K. H. Fornaçon, and K. H. Glassmeier, Institut für Geophysik und Extraterrestrische Physik, Technische Universität Braunschweig, Mendelssohnstrasse 3, D-38106 Braunschweig, Germany.

W. Baumjohann, K. Keika, W. Magnes, and R. Nakamura, Space Research Institute, Austrian Academy of Sciences, Schmiedlstrasse 6, A-8042 Graz, Austria. (kunihiro.keika@oeaw.ac.at)

C. M. Carr and E. A. Lucek, Space and Atmospheric Physics Group, Imperial College, South Kensington Campus, London SW7 2AZ, UK.

I. Dandouras, Centre d'Etude Spatiale des Rayonnements, Université Paul Sabatier, UMR 5187, CNRS, 9 Avenue du Colonel Roche, F-31028 Toulouse CEDEX 4, France.

M. Fillingim, Space Sciences Laboratory, University of California, 7 Gauss Way, Berkeley, CA 94720, USA.

G. D. Reeves, Los Alamos National Laboratory, 30 Bikini Atoll Road, Los Alamos, NM 87545, USA.

K. Yumoto, Space Environment Research Center, Kyushu University, 6-10-1 Hakozaki Higashi-ku, Fukuoka 812-8581, Japan.